Horizontal single-walled carbon nanotubes on MgO(110) and MgO(001) substrates

M. Maret, B. Saubat, J. Flock, A. Mantoux, F. Charlot, D. Makarov

Horizontal single-walled carbon nanotubes on MgO(1 1 0) and MgO(0 0 1) substrates

Mireille Maret [a,*], Bernadette Saubat [b], Johanna Flock [a], Arnaud Mantoux [a], Frédéric Charlot [c], Denys Makarov [d]

[a] Laboratoire de Science et Ingénierie des Matériaux et Procédés, Grenoble-INP/CNRS/UJF, BP 75, 38402 Saint-Martin d'Hères, France
[b] Laboratoire d'Electrochimie et Physico-Chimie des Matériaux et Interfaces, Grenoble-INP/CNRS/UJF, BP 75, 38402 Saint-Martin d'Hères, France
[c] Consortium des Moyens Technologiques Communs, Grenoble-INP, BP 75, 38402 Saint-Martin d'Hères, France
[d] Institute of Physics, Chemnitz University of Technology, D-09107 Chemnitz, Germany

Horizontal single-walled carbon nanotubes (SWNT) on MgO(1 1 0) and MgO(001) single-crystal sub-strates were synthesized in a temperature range of 830–910 °C by chemical vapor deposition using Co catalyst particles. SWNTs grow preferentially along the ⟨1 1 0⟩ directions of the two MgO surface planes. For synthesis at 830 °C, the distribution of the radial breathing mode (RBM) frequencies of SWNTs grown on MgO(11 0) is centered at 142 and 168 cm^{-1}, attributed to semi-conducting SWNTs. For the same syn-thesis time, the RBM distribution of SWNTs grown on MgO(0 01) is significantly broader. This difference would be due to the larger surface energy of MgO(11 0) which reduces the probability of coalescence between Co particles.

1. Introduction

Single-walled carbon nanotubes (SWNT) exhibit outstanding electrical and mechanical properties which make them potentially interesting as components for future electronic devices [1]. Therefore, numerous studies have been focused on the understanding of the growth mechanism of SWNTs in order to control size and chirality which determine their intrinsic transport properties [2]. An attractive synthesis process is the direct chemical vapor deposition method assisted by catalyst particles of regular size grown on single-crystal substrates. The lattice symmetry of the substrate can drive the horizontal growth of carbon nanotubes (CNT) along preferential crystallographic directions, as it was demonstrated on the A$(1\,1\,\bar{2}\,0)$ and R$(1\,\bar{1}\,0\,2)$ planes of sapphire substrates [3,4]. On the R surface using successively $^{13}CH_4$ and $^{14}CH_4$ gases, a base-growth mode of the aligned SWNTs was observed, highlighting the importance of the CNT–sapphire interactions [5]. This route for growing aligned CNT could be exploited for nanotube integration into circuits as transistors [6] or interconnects [7]. A recent development in the fabrication of NT-based devices was the direct growth of bent carbon nanotubes on sapphire substrates with artificial step structures [8]. The size of catalytic particles is also a crucial parameter since it controls the diameter of the nanotubes. An universal ratio between the diameters of the particle and the formed nanotube was found to be equal to 1.6 and was explained via a growth mechanism based on the formation of heptagon defects [9]. Furthermore, it was shown that the lattice symmetry could favor certain chiralities [10] and the atomic arrangements in the substrate planes could even induce unidirectional growth of CNTs [11]. On MgO(001) substrates, we have observed the horizontal growth of CNTs aligned preferentially along the two orthogonal directions [1 1 0] and $[1\,\bar{1}\,0]$ using carbon monoxide as feeding gas [12]. It is worth emphasizing that these two directions as well as the ones observed on the A and R planes of sapphire, namely the $[\bar{1}\,1\,0\,0]$ and $[\bar{1}\,1\,0\,\bar{1}]$, respectively, correspond to rows of pure oxygen atoms. Such oriented growth would thus be driven by the interactions between the growing carbon nanotubes and oxygen atoms of the substrate. The growth of horizontal straight micrometer-long nanotubes requires rather low density of catalysts on MgO(001). In contrast, for a high density of particles, vertically aligned carbon nanotubes were formed using ethylene, with lengths of a few millimeters [13].

In this Letter, we present for the first time the CVD synthesis of SWNTs on the (1 1 0) plane of MgO catalyzed by Co particles. We show that SWNTs are aligned preferentially along the unique favorable direction $[1\,\bar{1}\,0]$. For comparison, syntheses of SWNTs on MgO(1 1 0) and MgO(0 0 1) surfaces were performed simultaneously. From the frequencies of the radial breathing mode (RBM) observed in the Raman spectra, the distribution of the diameters of SWNTs grown on MgO(1 1 0) is found to be substantially narrower than on MgO(0 0 1).

2. Experimental

Deposition of a thin layer of Co with a nominal thickness of about 1 Å was performed at 430 °C simultaneously on MgO(1 1 0) and MgO(0 0 1) substrates (size of $10 \times 10 \times 0.5\ mm^3$) in an

* Corresponding author.
E-mail address: mireille.maret@simap.grenoble-inp.fr (M. Maret).

ultra-high-vacuum chamber (base pressure of 2×10^{-10} mbar). The flux of Co atoms emitted from an e-gun source corresponds to a deposition rate of 0.01 Å/s. The magnesium oxide has a cubic NaCl-type structure with Mg and O atoms arranged in the (001) and (110) planes as shown in Fig. 1. The ⟨110⟩ directions correspond to alternate rows of pure O and pure Mg atoms.

After deposition, the samples with self-assembled Co nanoparticles were examined under ambient conditions by atomic force microscopy (AFM) in tapping mode using a Veeco 3100 apparatus. Typical AFM images are shown in Fig. 2. The root mean square (RMS) roughnesses are equal to 0.3 and 0.5 nm on the (001) and (110) surfaces, respectively. The larger roughness found on MgO(110) is mainly related to the presence of a few holes of 1 nm depth. The self-assembled Co particles are somewhat difficult to separate from the nanograins of MgO. Nevertheless, examination of line profiles (insets in Fig. 2) has allowed us to estimate the average height of Co particles equal to 1.4 ± 0.5 nm with a separation distance of 35 ± 5 nm.

Both MgO substrates with Co deposits were cleaved into smaller pieces of 3×3 mm^2 and stored in an evacuated dessicator to preserve the samples from humidity. For each synthesis, one piece of MgO(001) and one piece of MgO(110) were placed on an alumina support, which was centered inside a horizontal quartz tube reactor under atmospheric pressure. First, the tube was flowed with He, then He was exchanged with hydrogen with a flux of 100 sccm and the furnace was heated up to 580 °C. Waiting time of 1 h at 580 °C was applied to reduce Co oxide. Then the furnace was heated up to the synthesis temperature, at which the H_2 flow rate was reduced down to 20 sccm and the CO was introduced up to a flow rate of 80 sccm. Different temperatures of synthesis ranging from 830 to 910 °C were chosen. For each temperature the reaction time was fixed on 1 h. After this time, the CO/H_2 mixture was exchanged with helium and the furnace was cooled down to room temperature.

The MgO pieces with CNTs were examined using a Zeiss Ultra 55 field emission scanning electron microscope (FESEM) based on GEMINI e-Beam column technology. This equipment is well-suited for visualizing alignement of CNTs on a large scale. Imaging with the in-lens detector, which collects secondary electrons (SE) emerging from the uppermost part of sample, allows to visualize efficiently the carbon nanotubes. In contrast, imaging with the Everhart–Thornley (ET) detector, which collects under lower angles secondary electrons produced by both incident and backscattered electrons, reveals better the catalytic particles. In some cases, the images using ET detector have a better contrast than those taken using the backscattered electron in-lens (BSE) detector. Because of the charge effects induced by the insulating MgO susbtrate, a voltage of 1 kV was used. The diameters of carbon nanotubes and Co particles were then measured by atomic force microscopy.

Furthermore, single-walled carbon nanotubes were characterized by Raman spectroscopy. The spectra were collected with a Renishaw InVia Raman microscope equipped with an air-cooled ultra low noise detector in a backscattering configuration. An excita-

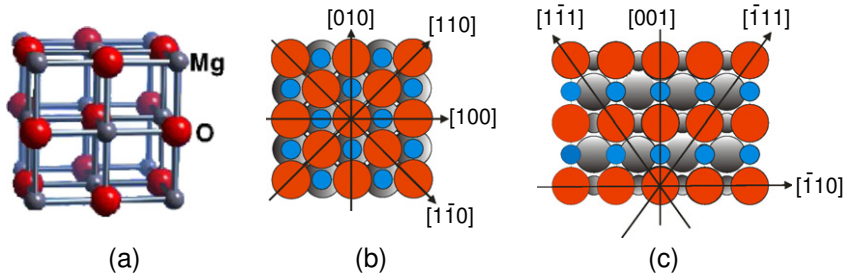

Fig. 1. The cubic NaCl-type crystal structure of magnesium oxide (a). Positions of the Mg and O atoms on the (001) (b) and (110) (c) planes. The red and blue circles represents the oxygen and magnesium atoms, respectively, arranged in the uppermost layer; the grey circles correspond to the atoms in the first underlayer.

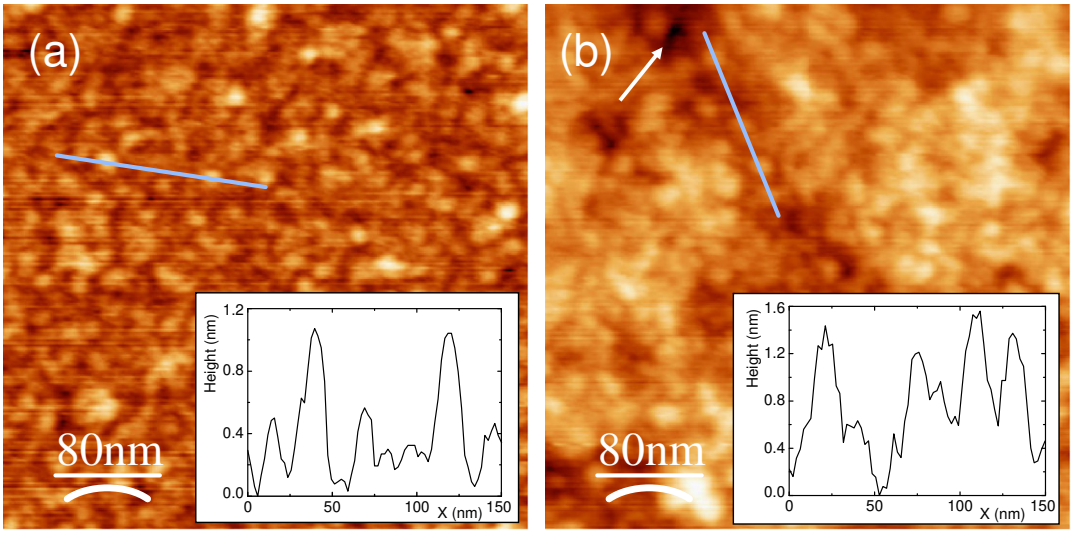

Fig. 2. AFM topography images of nominally 1-Å-thick Co deposits on MgO(001) (a) and MgO(110) (b). Insets reveal typical line profiles through Co particles. The white arrow marks a hole of 1 nm depth in MgO(110).

tion wavelength of 514.5 nm (E_i = 2.41 eV) from an Argon-ion laser focused on the surface through a 50× (NA = 0.95) objective (∼1 μm^2 spot size and 5 mW laser power) was used. Sets of spectra were recorded by rastering the samples in 1 μm steps.

3. Results and discussion

The carbon nanotubes grown on the two different planes of MgO were first characterized by FESEM. Fig. 3 shows the results of two CVD syntheses performed at 910 and 860 °C on MgO(001). In spite of different lengths and densities of CNTs on the two MgO substrates, the CNTs prefer to grow horizontally along the [110] and [1$\bar{1}$0] perpendicular directions. Other growth directions are detected for the sample synthesized at 910 °C and can be explained as follows: if an initially well-oriented growing nanotube hits other Co particles or CNTs, these obstacles as well as defective areas of the MgO surface will strongly damp the lattice-induced growth and will deviate the CNT from its initial growth direction. While a single family of CNTs of about 1 μm length is observed in Fig. 3a, two families are revealed in Fig. 3b–d. Besides a few long and oriented nanotubes lying on the surface, other nano-objects, rather embedded in the surface and also oriented along the ⟨110⟩ directions, are detected by the SE (ET) detector (Fig. 3d). As shown later, these nano-objects were clearly identified by AFM as nanotubes. Most of the short nanotubes are ended at Co particles, which correspond to dark dots while measuring with the SE in-lens detector (Fig. 3c) or bright dots with the SE (ET) sideways detector (Fig. 3d).

Fig. 4 shows the FESEM images obtained for the two pieces of Mg(110) after synthesis at 910 and 860 °C. For the synthesis at 910 °C (Fig. 4a) 1 μm long CNTs are observed, preferentially oriented along the [1$\bar{1}$0] direction in the (110) plane. However, other growth directions as the ⟨111⟩ ones exist. Similar to the MgO(001) sample, no CNTs are oriented along the ⟨100⟩ directions. Fig. 4b–d shows FESEM images of the MgO(110) sample after synthesis at 860 °C. Images (b–d) in Fig. 4, recorded using three different detectors, correspond to the same region of MgO(110) sample. In spite of numerous recrystallized regions revealed by the SE (ET) detector (Fig. 4c), two families of CNTs were formed preferentially located on the flat regions (bright areas in Fig. 4d) elongated along the [1$\bar{1}$0] direction. The first family is well-imaged by the SE in-lens detector and is likely located above the MgO surface (Fig. 4b). The second one consists of shorter nanotubes lying on the flat areas: a few CNTs are visible in Fig. 4c. The recrystallized areas could be induced by H_2O vapor formed during the synthesis according to the reaction: $CO + H_2 \leftrightarrow C + H_2O$, together with the disproportionation of CO. The mobility of Co particles and thus the importance of coalescence effects are expected to be quite different on the flat and recrystallized regions with various roughnesses. As shown from numerous experimental and theoretical studies [9,14–16], the particle size determines the nanotube diameter but, as noticed by Paillet et al. [17], the particle diameter is sometimes only an upper limit for the produced nanotube diameter. Two families of nanotubes are observed on both MgO(001) and MgO(110) surfaces after synthesis at 860 °C. The shorter tubes well-oriented along the ⟨110⟩ directions have grown on flat areas of MgO substrates from rather large Co particles. In contrast, the longer nanotubes lying rather above the surface and adopting different directions have grown from small Co particles located preferentially on damaged areas of MgO.

AFM observations of CNTs and Co particles are shown in Fig. 5. Images (a) and (b) were taken for the same MgO(001) samples as shown in Fig. 3. The diameters of the visualized nanotubes vary between 1.1 and 6 nm, and the heights of the Co particles between 1.5 and 7 nm (Fig. 5a). During the synthesis time of 1 h, the inactive Co particles merge to form the large particles as visualized by AFM. Fig. 5b confirms that the objects in close contact with the substrate, observed by FESEM (Fig. 3d), are carbon nanotubes. Such nanotubes have large diameters up to 10 nm. Large particles can even give rise to two nanotubes as shown in the inset of Fig. 5b. All these short and straight nanotubes are aligned along one of the two per-

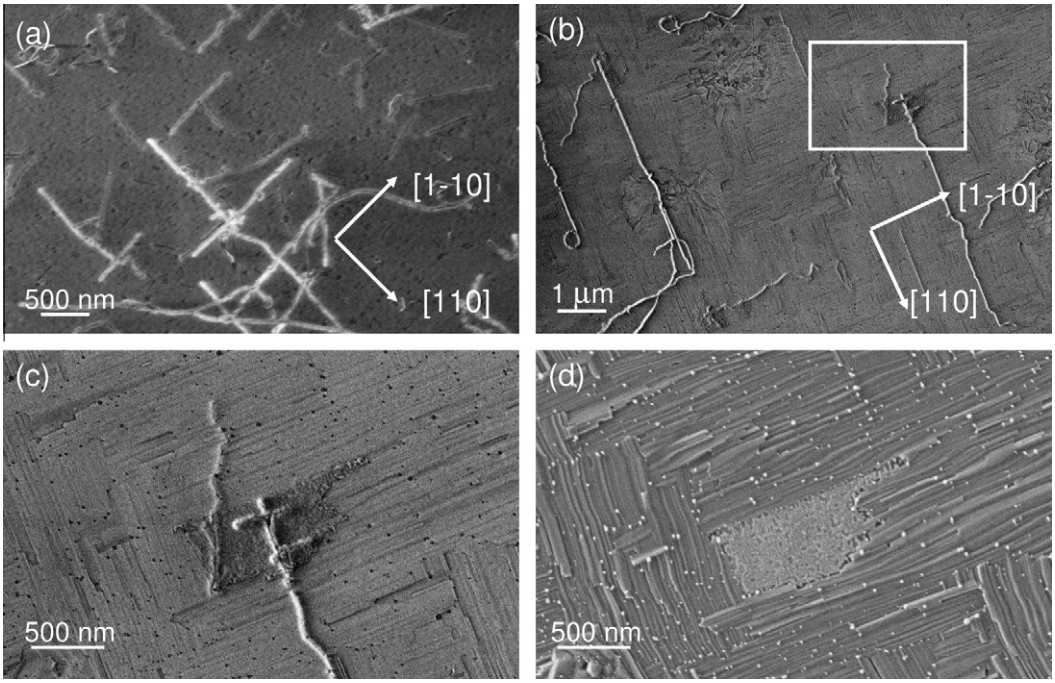

Fig. 3. FESEM images of carbon nanotubes grown on MgO(001) by CVD of a CO/H_2 mixture. CNTs grow along the [110] and [1$\bar{1}$0] preferential directions. (a) Synthesis at 910 °C. (b–d) Synthesis at 860 °C: (c) and (d) are higher magnification images of the area defined by the white square in (b). Images (a–c) were recorded by the SE in-lens detector and image (d) by the SE (ET) detector revealing the Co catalyst particles.

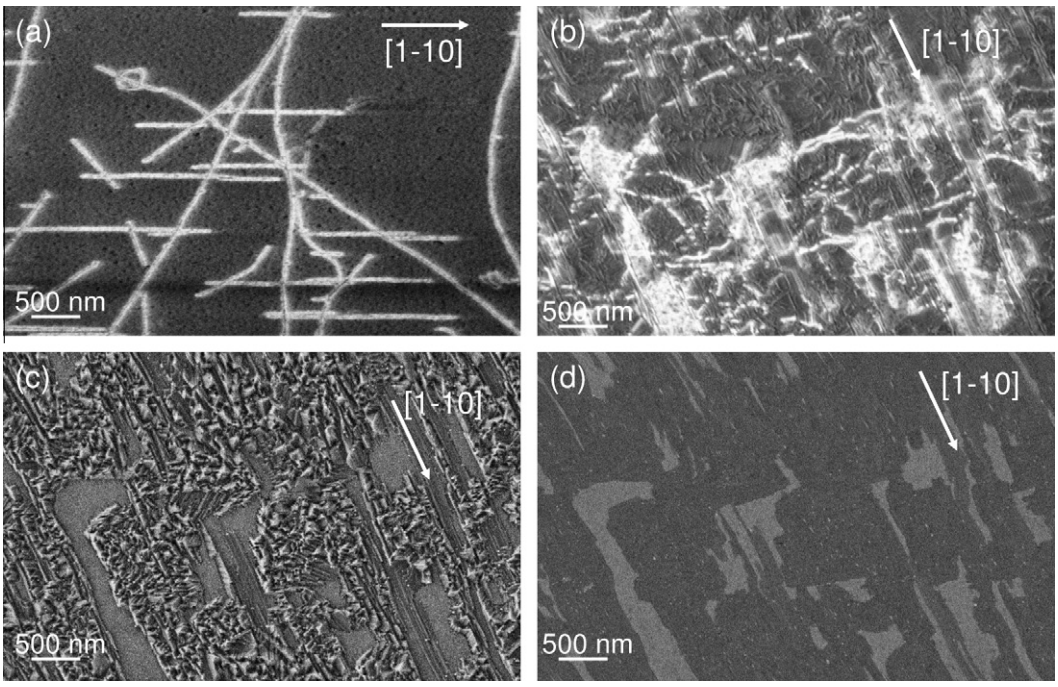

Fig. 4. FESEM images of carbon nanotubes grown on MgO(1 1 0) by CVD of a CO/H_2 mixture. CNTs grow along the [1 $\bar{1}$ 0] preferential direction. (a) Synthesis at 910 °C. (b–d) Synthesis at 860 °C: (b–d) images correspond to the same area. Carbon nanotubes are clearly identified by the SE in-lens detector (a and b). Image (c) was recorded by the SE (ET) detector, revealing the recrystallization of the MgO surface. Image (d) by the BSE in-lens detector showing some strips oriented along the [1 $\bar{1}$ 0] direction, whose contrast is not chemical but related to the different surface states.

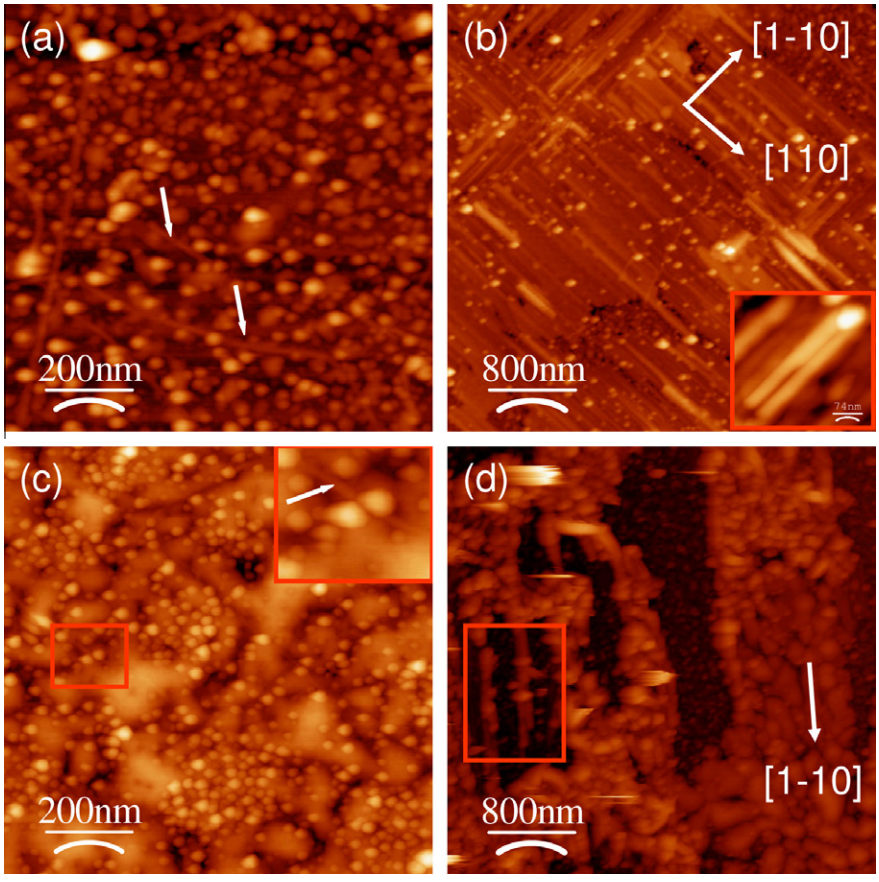

Fig. 5. AFM topography images of carbon nanotubes grown on MgO(0 0 1) at 910 °C (a) and 860 °C (b) and on MgO(1 1 0) at 830 °C (c) and 860 °C (d). SWNT of ~1 nm diameter are indicated by white arrows in (a). In images (b) and (d) the visualized carbon nanotubes are well-aligned along the indicated crystallographic directions of the MgO substrate. The inset in (c) shows a high magnification image of a CNT with a diameter of about 1 nm.

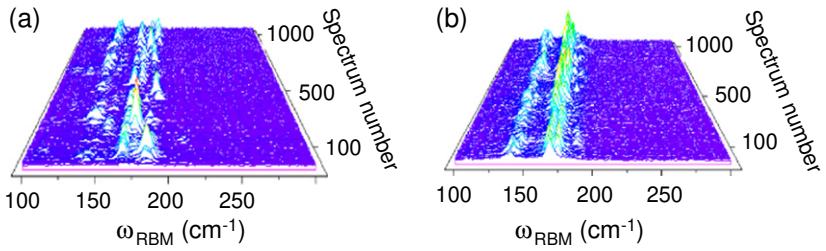

Fig. 6. Series of 1050 RBM Raman spectra, recorded while rastering the samples in a 1 μm step on an area of ~30 × 35 μm². CVD syntheses at 830 °C on MgO(001) (a) and MgO(110) (b).

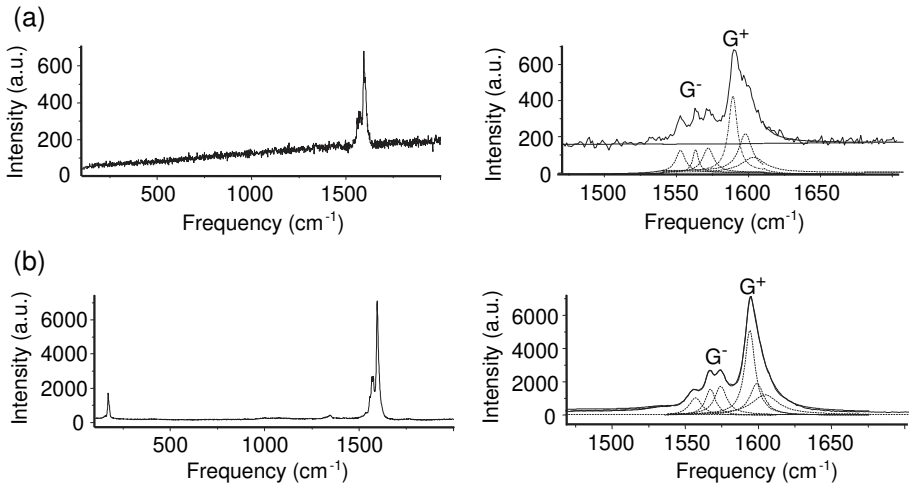

Fig. 7. Typical Raman spectra of SWNTs obtained after CVD synthesis at 860 °C on MgO(001) (a) and MgO(110) (b). The G^- and G^+ tangential bands can be decomposed into three components of lorentzian shape, for G^- centered at 1556, 1567 and 1575 cm^{-1} and G^+ at 1594, 1599 and 1605 cm^{-1}.

pendicular directions ⟨110⟩. It is worth noting that some large particles are located above the short nanotubes. Fig. 5c and d are AFM images recorded on the MgO(110) pieces after synthesis at 830 and 860 °C. Unfortunately, no AFM image could be taken for the sample shown in Fig. 4a. In comparison with the AFM images measured just after Co deposition (Fig. 2c and d), the surface state of the two MgO(110) pieces has changed. In Fig. 5c, the diameters of the CNTs grown at 830 °C are in the range of 1–3 nm, and the Co particles with height in the range of 4–6 nm are distributed around the broad MgO grains. The change of the MgO surface is more pronounced after the synthesis at 860 °C, which corresponds to a surface recrystallization. Such modification limits substantially the horizontal oriented growth of CNTs driven by the lattice symmetry. Nevertheless, on flat and elongated substrate areas a preferential growth along the $[1\bar{1}0]$ direction is well observed, as shown by the two nanotubes (Fig. 5d, red[1] rectangle) with diameters of about 15 nm.

The existing RBM frequencies in the Raman spectra confirm the growth of single-walled carbon nanotubes on both surfaces for synthesis temperatures ranging from 830 to 910 °C. Fig. 6 shows the maps constructed from a thousand spectra recorded on ~30 × 35 μm² areas of MgO(001) and MgO(110) after synthesis at 830 °C. Most of the measured RBM frequencies, ω_{RBM}, vary from 120 to 190 cm^{-1}, corresponding to SWNT with diameters, d, from 2.2 down to 1.2 nm, based on the relation established for free-standing SWNTs: $\omega_{RBM} = A/d + B$ with $A = 204\ cm^{-1}$ and $B = 27\ cm^{-1}$ [18]. On MgO(110) surface, the distribution of the RBM frequencies is centered at two values, 142 and 168 cm^{-1}, which corresponds to a distribution of diameters of CNTs centered at 1.75 and 1.45 ± 0.5 nm, respectively. From the so-called Kataura plot [19], taking into account the excitation energy of 2.41 eV, these two families of resonantly probed SWNTs are semi-conducting in agreement with their general TM mode lineshape. Attempts to probe metallic SWNTs with diameters in the range of 1.45–1.75 nm using a laser excitation line of 785 nm (1.58 eV) has failed due to strong MgO fluorescence. On the MgO(001) surface, the double distribution is not well pronounced and could be related to a higher mobility of the Co particles, favored by the surface energy of MgO(001), which is twice smaller than the one of MgO(110) [20]. Consequently, coalescence probability between Co particles is increased leading to a broad range of particle diameters and accordingly to various diameters of SWNTs. In addition to semi-conducting SWNTs, a few metallic SWNTs were also identified, characterized by a large G^- lineshape and a RBM frequency in the range of 120–125 cm^{-1} corresponding to diameters close to 2 nm. The RBM frequency distribution measured for the samples synthetized at 860 °C was found to be broader on MgO(001) and MgO(110). This feature can be attributed to a larger range of Co particle diameters resulting from the damage of the MgO substrates as discussed above.

Several Raman spectra display a unique narrow (6–7 cm^{-1}) RBM line and well-resolved TM modes suggesting signals coming from individual SWNTs. As shown in Fig. 7, for SWNTs synthetized at 860 °C, a closer examination of the G^- bands reveals a triplet structure. Such feature also appears in the spectrum of the MgO(001) sample, which presents no RBM mode and weak intensities of the G bands characteristic of less-resonant conditions. The three components are well-fitted by lorentzians, with maxima at

[1] For interpretation of color in Figs. 1 and 5, the reader is referred to the web version of this article.

1556, 1567 and 1575 cm^{-1} and widths in the range of 5–10 cm^{-1}. A triplet structure feature is also observed for the G^+ band, but contrary to the G^- band case, the splitting is less pronounced with a separation of only 4–5 cm^{-1}. Nevertheless, for few spectra exhibiting very narrow widths of individual components, the G^+ band was successfully fitted by three lorentzians centered at 1594, 1599 and 1605 cm^{-1}. These narrow linewidths are attributed to well-crystallized nanotubes with few structural defects. Such good crystalline state is supported by the weak intensity or even the absence of the D band at 1340 cm^{-1}.

According to previous reports based on a group theory analysis [21,22], these six modes occur for chiral SWNTs and correspond to two A_1, two double degenerate E_1 and two double degenerate E_2 symmetry modes with atomic vibrations either along the tube axis direction or along the circumferential direction [23]. The measured spectra show that the TM component with the highest frequency has a low intensity and, in agreement with theoretical calculations, can be attributed to a E_2 mode. Similar consideration allows us to attribute an E_2 symmetry to the lowest frequency mode. Full polarized Raman studies are nevertheless required to assign the A_1 and E_1 symmetry modes to other components.

4. Conclusion

We have demonstrated the feasability of growing horizontal SWNTs by CVD, preferentially along the $[1\bar{1}0]$ direction on the MgO(110) surface, using a CO/H_2 mixture and Co self-assembled catalyst particles. On MgO(001) we confirm the two preferential growth directions [110] and $[1\bar{1}0]$, also observed for dense assemblies of CNTs. Compared with the MgO(001) substrate, the larger surface energy of MgO(110) reduces the coalescence effects between Co particles and consequently leads to a narrow distribution of SWNT diameters. For synthesis at 830 °C, the diameters of the probed semi-conducting SWNTs on MgO(110) are centered at 1.45 and 1.75 nm. In order to grow perfectly parallel and long straight SWNTs on MgO(110), further improvement in the synthesis procedure is needed, focussed on the preservation of the good surface state of MgO and the location of catalytic particles on restricted areas.

Acknowledgements

The authors thank P. Gadelle (SIMaP) for enlightening discussions and Prof. M. Albrecht (TU Chemnitz) for the given opportunity to perform deposition of Co thin films.

References

[1] M.S. Dresselhaus, G. Dresselhaus, P. Avouris, Carbon nanotubes, Topics in Applied Physics, vol. 20, Springer-Verlag, Berlin, 2001.
[2] A. Loiseau, P. Launois, P. Petit, S. Roche, J.P. Salvetat, Understanding carbon nanotubes, Lect. Notes Phys., vol. 677, Springer, Berlin/Heidelberg, 2006.
[3] S. Han, X. Liu, C. Zhou, J. Am. Chem. Soc. 127 (2005) 5294.
[4] H. Ago, K. Nakamura, K. Ikeda, N. Uehara, N. Ishigami, M. Tsuji, Chem. Phys. Lett. 408 (2005) 433.
[5] H. Ago et al., J. Phys. Chem. C 112 (2008) 1735.
[6] A. Bachtold, P. Hadley, T. Nakanishi, C. Dekker, Science 294 (2001) 1317.
[7] A. Naeemi, J.D. Meindl, Annu. Rev. Mater. Res. 39 (2009) 255.
[8] H. Ago, K. Imamoto, T. Nishi, M. Tsuji, T. Ikuta, K. Takahashi, M. Fukui, J. Phys. Chem. C 113 (2009) 13121.
[9] A.G. Nasibulin, P.V. Pikhitsa, H. Jiang, E.I. Kauppinen, Carbon 43 (2005) 2251.
[10] N. Ishigami, H. Ago, K. Imamoto, M. Tsuji, K. Iakoubovskii, N. Minami, J. Am. Chem. Soc. 130 (2008) 9918.
[11] N. Ishigami, H. Ago, T. Nishi, K.I. Ikeda, M. Tsuji, T. Ikuta, K. Takahashi, J. Am. Chem. Soc. 130 (2008) 17264.
[12] M. Maret, K. Hostache, M.C. Schouler, B. Marcus, F. Roussel-Dherbey, M. Albrecht, P. Gadelle, Carbon 45 (2007) 180.
[13] G.Y. Xiong, D.Z. Wang, Z.F. Ren, Carbon 44 (2006) 969.
[14] Y. Li, W. Kim, Y. Zhang, M. Rolandi, D. Wang, H. Dai, J. Phys. Chem. B 105 (2001) 11424.
[15] S. Han et al., J. Phys. Chem. B 108 (2004) 8091.
[16] J.C. Burgos, H. Reyna, B.I. Yakobson, P.B. Balbuena, J. Phys. Chem. C 114 (2010) 6952.
[17] M. Paillet, V. Jourdain, P. Poncharral, J.L. Sauvajol, A. Zahad, J. Phys. Chem. B 108 (2004) 17112.
[18] J.C. Meyer et al., Phys. Rev. Lett. 95 (2005) 217401.
[19] H. Kataura, Y. Kumazawa, Y. Maniwa, I. Umezu, S. Suzuki, Y. Ohtsuka, Y. Achiba, Synth. Met. 103 (1999) 2555.
[20] V.E. Henrich, P.A. Cox, The Surface Science of Metal Oxides, Cambridge University Press, Cambridge, 1994. p. 36.
[21] R.A. Jishi, L. Venkataraman, M.S. Dresselhaus, G. Dresselhaus, Chem. Phys. Lett. 209 (1993) 77.
[22] M.S. Dresselhaus, G. Dresselhaus, R. Saito, A. Jorio, Phys. Rep. 409 (2005) 47.
[23] D. Khan, J.P. Lu, Phys. Rev. B 260 (1999) 6535.